Available online at www.sciencedirect.com
SCIENCE DIRECT®
Journal of Power Sources 123 (2003) 230–240
JOURNAL OF POWER SOURCES
www.elsevier.com/locate/jpowsour

Mathematical modeling of the capacity fade of Li-ion cells

P. Ramadass, Bala Haran, Ralph White, Branko N. Popov*
Department of Chemical Engineering, University of South Carolina, Columbia, SC 29208, USA

Received 14 March 2003; accepted 29 March 2003

Abstract

A capacity fade prediction model has been developed for Li-ion cells based on a semi-empirical approach. Correlations for variation of capacity fade parameters with cycling were obtained with two different approaches. The first approach takes into account only the active material loss, while the second approach includes rate capability losses too. Both methods use correlations for variation of the film resistance with cycling. The state of charge (SOC) of the limiting electrode accounts for the active material loss. The diffusion coefficient of the limiting electrode was the parameter to account for the rate capability losses during cycling.

Keywords: Capacity fade model; Li-ion batteries; Semi-empirical model; Cycle life

1. Introduction

Li-ion batteries have replaced Ni–MH and Ni–Cd systems for several applications that require high power densities. Numerous studies have reported the capacity fade of these batteries under extended cycling. For aerospace and other advanced applications, it is essential to quantify the capacity loss for a given cycling protocol. Real-time cycle life testing becomes prohibitively expensive if one considers the number of different variables that can change such as depth of discharge (DOD), charge and discharge rates and cycling temperature. Thus, accelerated cycle life testing and developing correlations based on this data becomes very critical for estimation of the capacity fade of the cell.

Bloom et al. [1] reported accelerated calendar and cycle life study of 18,650 cells. Useful life according to these authors was strongly affected by temperature, time, state of charge (SOC) and change in state-of-charge (ΔSOC). To estimate the percentage of power loss the data were fit with the general equation:

$$Q = A \exp\left(\frac{-E_a}{RT}\right) t^z \tag{1}$$

where Q represents the percentage power loss, t (weeks) the time, T (K) the temperature, A the pre-exponential factor, E_a (J) the activation energy, and z the adjustable parameter. Similarly, Inoue et al. [2] used the calendar life data to predict the cycle life of the battery. According to these authors the corrected cycling capacity loss data correlated linearly with the cell internal resistance. The above models are empirical in nature and do not present any insight into the processes that contribute to the capacity and rate capability losses during cycling.

The capacity fade and prediction of the battery discharge characteristics with cycling could be obtained by using a semi-empirical approach or by developing a first principles model. A survey of the literature indicates that for other battery systems capacity fade analysis has relied on developing empirical correlations that are specific to the experimental conditions. Hafen and Corbett [3] developed an empirical correlation for cycle life prediction of Ni–Cd cells based on the experimental cycling data. The cycle of Mth failure has been derived as

$$\text{cycle}\,|_{M\text{th failure}} = 9.71 \left(\frac{M}{N}\right)^{0.229} (\text{DOD})^{-1.545} \times \exp\left\{\frac{3843}{T(\text{K})}\right\} \tag{2}$$

where N is the number of cells in battery and DOD is the depth of discharge.

Bro and Levy [4] developed an Arrhenius type relation to explain the capacity loss of Li–$SOCl_2$ cells with storage time and aging temperature, which is expressed as

$$C(t, T) = C_0 - k_0 t e^{-(E/RT)} \tag{3}$$

where $C(t, T)$ is the capacity loss at time 't' and temperature 'T' and the capacity loss at $t = 0$ is defined as $C_0 = 0$.

* Corresponding author. Tel.: +1-803-777-7314; fax: +1-803-777-8265.
E-mail address: popov@engr.sc.edu (B.N. Popov).

0378-7753/$ – see front matter © 2003 Elsevier Science B.V. All rights reserved.
doi:10.1016/S0378-7753(03)00531-7

Nomenclature

a	specific surface area of porous electrode (m^2/m^3)
c	concentration of Li or Li^+ ions (mol/m^3)
D	diffusion coefficient (m^2/s)
F	Faraday's constant, 96,487 (C/mol)
i_0	exchange-current density (A/m^2)
i_{app}	applied current density ($16.54\ A/m^2$)
J	local volumetric current density (A/m^3)
k	rate constant of electrochemical reaction ($(A/m^2)/(mol/m^3)^{3/2}$)
L	length of the cell (m)
MW	molecular weight (mol/kg)
N	cycle number
Q	capacity (mAh)
r	radial coordinate (m)
R	particle radius (μm)
R_f	film resistance at the electrode–electrolyte interface ($\Omega\ m^2$)
R_g	universal gas constant, 8.314 (J/mol)
t	time (s)
t^+	transference number of Li^+ ions in the electrolyte
T	temperature (K)
U	local equilibrium potential (V)
x	coordinate across the cell thickness (m)

Greek letters

α_a, α_c	anodic and cathodic transfer coefficients of electrochemical reaction
ε	volume fraction of a phase
ϕ	local potential of a phase (V)
η	local over-potential driving electrochemical reaction (V)
κ	conductivity of electrolyte (S/m)
θ	state-of-charge
σ	conductivity of electrode (S/m)
ρ	density of active material (kg/m^3)

Subscripts

1	solid phase
2	solution phase
n	negative
N	cycle number
p	positive
s	separator
th	theoretical

Superscripts

o	initial
eff	effective
max	theoretical maximum
ref	reference

The parameters namely acceleration factor, 'k_0'and activation energy 'E' were obtained from the least squares fit from a plot of the logarithm of the capacity loss obtained experimentally versus inverse of the aging temperature.

Researchers at SAFT [5] developed a life duration model for the Ni–MH cells that involves an empirical correlation for rate of corrosion given as

$$\frac{\partial_{\text{corrosion}}(t, T, \%)}{\partial t} = f\left(\frac{\partial e}{\partial t}, \frac{\partial S}{\partial t}, e, S, E_a\right) \quad (4)$$

where t is the time, T the cell temperature, percentage denotes the discharged capacity, S the initial alloy surface area, E_a the activation energy and e the thickness of the corrosion layer. In this paper, we plan to adopt a similar approach to derive semi-empirical correlations for the capacity fade of Li-ion battery systems. The main drawback of this methodology is its system specific nature. In other words, the semi-empirical correlations developed for one type of Li-ion cell of specific geometry and electrode material need not be the same for other type. Even though the parameters considered for capacity loss may be common for all Li-ion systems, the trend in the variation of these parameters with continuous cycling may not be the same. Thus, in order to develop a mathematical model for capacity fade, it is critical to understand the various mechanisms involved in capacity loss. Our previous research on Li-ion systems of different geometries, cathode materials and varying cycling conditions resulted in a better understanding of the capacity fade mechanisms involved in each of the systems studied [6,7].

This paper primarily focuses on developing semi-empirical correlations to account for the capacity fade in Li-ion cells. We analyzed the performance of 18,650 cells as a function of number of cycles in order to develop semi-empirical correlations for the state of charge (reversible lithiation capacity) and the battery resistance (film and polarization resistance) as a function of number of cycles.

Previously, based on the performance data (charge and discharge characteristics) and the destructive physical analysis (DPA) of fresh and cycled electrode materials, we identified the main factors responsible for capacity fade of Li-ion systems with cycling [8,9]. According to our analysis, the capacity fade can be split into three components. The first part deals with the loss in capacity due to increase in resistance at both electrodes. The second part deals with loss of lithiation capacity at both electrodes. The third part arises due to loss of active material Li^+ in the cell. Any model that will be used to analyze the capacity fade has to account for capacity losses due to these three terms. In this paper, we follow changes in state of charge, film resistance and diffusion coefficient to quantify the capacity fade. The state of charge accounts for the active material loss (both primary and secondary active material) while the film resistance controls the drop in the cell voltage with continuous cycling. Since the rate capability loss is due to transport limitations induced with cycling by formation of oxide layers on both electrodes, the solid phase diffusion coefficient of the limiting electrode

was considered as parameter to account for the rate capability losses. Discharge curves at different cycles were fitted to first principles model. From this fitting, semi-empirical correlations were developed which account for the variation of the three parameters and hence the battery capacity fade with cycling. These correlations were used along with a first principles based dual Li-ion intercalation model to simulate the performance of the Li-ion cell at different discharge rates.

2. Experimental

All experimental data that includes full-cell and half-cell studies for developing the semi-empirical models were obtained from our previous work on capacity fade studies of Li-ion cells cycled at elevated temperatures [8,9]. A brief overview of the experimental work is included here for clarity. Sony 18,650 cells with 1.8 Ah rated capacity were used for all cycling studies. For charging the cells, the conventional constant current–constant voltage (CC–CV) protocol was adopted. A direct current of 1 A is used to charge the cell during the constant current part and the cut off voltage was set to be 4.2 V. Subsequently the voltage was held constant at 4.2 V till the current drops to 50 mA. Charge–discharge studies were carried out in the potential range of 2.0–4.2 V. Arbin BT-2000 battery cycler has been used for all cycling studies. Three cycle numbers 150, 300 and 800 were chosen to analyze the cycled cells. Rate capability studies were performed for the fresh cell as well as for the cycled cells. The cells were charged using the same CC–CV protocol as used for the cycling studies followed by discharging at different rates ($C/9$ to $1C$). The following studies were performed on the individual electrodes of the cell. The can of cycled Sony US18650S cells was carefully opened at fully discharged state in a glove box filled with ultra pure argon. Next, pellet or disc electrodes were made from the positive and negative electrodes of Sony 18650 cell and were used as working electrodes in the T-cell. Pure lithium metal was used as the counter and as reference electrode. Pellet electrodes from the cells after different cycles were cycled at very low rates ($\sim C/15$) and the intrinsic capacity of both positive and negative electrode was determined. The difference in capacity between the first cycle and the present cycle yields the loss in lithiation capacity at both electrodes.

2.1. The Li-ion intercalation model

Fig. 1 shows a schematic representation of a typical Li-ion cell consisting of three regions namely negative electrode (graphite), separator (poly-propylene) and positive electrode ($LiCoO_2$). Both the graphite and $LiCoO_2$ are porous composite insertion electrodes. During discharge, the lithium ions de-intercalate from the negative electrode and intercalates into the positive electrode through a highly conductive electrolyte solution. As a result of discharge, the cell voltage decreases since the equilibrium potentials of the two electrodes depend on the lithium concentration on the surface of the electrode particles. During charging of Li-ion cells the reverse reactions occur. To explain these phenomena mathematically, one needs to consider model equations that describe, mass transport of lithium in solid phases, mass transport of lithium ions in the solution phase, charge

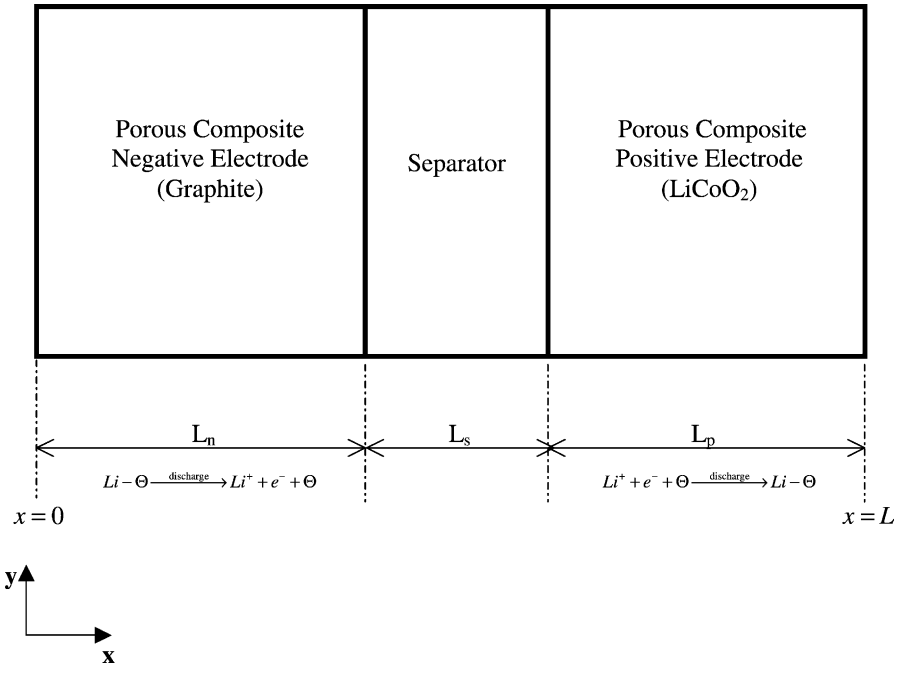

Fig. 1. Schematic of a typical Li-ion cell sandwich.

transport in the solid phases and charge transport in the solution phase [10,11].

The governing equations for potential distribution in solid and solution phases were

$$\nabla \cdot (\sigma^{\text{eff}} \nabla \phi_1) - J = 0 \tag{5}$$

$$\nabla \cdot (\kappa^{\text{eff}} \nabla \phi_2) + \nabla \cdot (\kappa_{\text{D}} \nabla \ln c_2) + J = 0 \tag{6}$$

respectively, where the appropriate definitions for effective conductivities (σ^{eff}, κ^{eff}) and the diffusional conductivity (κ_{D}) were given in detail in [10,11]. The model equation that describes the solid phase lithium concentration is given by

$$\frac{\partial c_{1,j}}{\partial t} = \frac{\text{D}_{1,j}}{r^2} \frac{\partial}{\partial r} \left(r^2 \frac{\partial c_{1,j}}{\partial r} \right), \quad j = \text{n, p} \tag{7}$$

and for explaining the mass transport of lithium ions in the solution phase the following equation used was

$$\varepsilon_2 \frac{\partial c_2}{\partial t} = \nabla \cdot (D_2^{\text{eff}} \nabla c_2) + \frac{1 - t^+}{F} J \tag{8}$$

The equations describing the electrochemical reactions, mass transport, and other physical processes within the cell are discussed in detail in [10–12].

Butler–Volmer kinetic expression was used to describe the charge transfer processes occurring across both the electrode–electrolyte interfaces. Thus, the local volumetric transfer current density due to charge transfer is given by

$$J = a_j i_{0,j} \left[\exp\left(\frac{\alpha_{\text{a},j} F}{RT} \eta_j \right) - \exp\left(-\frac{\alpha_{\text{c},j} F}{RT} \eta_j \right) \right], \quad j = \text{n, p} \tag{9}$$

where $i_{0,j}$ is the concentration dependent equilibrium exchange current density at an interface and is given by

$$i_{0,j} = k_j (c_{1,j}^{\max} - c_{1,j}^{\text{s}})^{\alpha_{\text{a},j}} (c_{1,j}^{\text{s}})^{\alpha_{\text{c},j}} (c_2)^{\alpha_{\text{a},j}}, \quad j = \text{n, p} \tag{10}$$

The over-potential for the intercalation reaction can be expressed as

$$\eta_j = \phi_1 - \phi_2 - U_{j,\text{ref}} - \frac{J}{a_{\text{n}}} R_{\text{f}}, \quad j = \text{n, p} \tag{11}$$

The equilibrium potentials ($U_{j,\text{ref}}$) of positive and negative electrode are expressed in terms of functions of state-of-charge:

$$\begin{aligned} U_{\text{p}}^{\text{ref}} &\rightarrow f(\theta_{\text{p}}) \\ U_{\text{n}}^{\text{ref}} &\rightarrow f(\theta_{\text{n}}) \end{aligned} \tag{12}$$

Fig. 2 presents the open circuit potential (OCP) curves of positive and negative electrodes of Li-ion cells obtained experimentally using a T-cell assembly with pure Li metal foil as counter and reference electrode where the electrode materials were subjected to a very low rate lithiation. The empirical expressions (Eqs. (A.1) and (A.2)) that represent the variation of U_j^{ref} as a function of θ_j were obtained from fitting the experimental data. The same empirical relations were used for all cycling simulations of semi-empirical models presented in this paper.

The design adjustable parameters and other parameters for the electrodes that are necessary for the model are given in Table 1. This nonlinear system of five independent governing equations and five dependent variables (c_1, c_2, ϕ_1, ϕ_2, J) is solved as a 1D–2D coupled model for the three domains (negative/separator/positive) using FEMLAB software.

In general, the theoretical specific capacity of any electrode material could be calculated based on Faraday's law that can be expressed as

$$Q_{\text{th},i}(\text{As/g}) = \frac{F}{\text{MW}_i}, \quad i = \text{n, p} \tag{13}$$

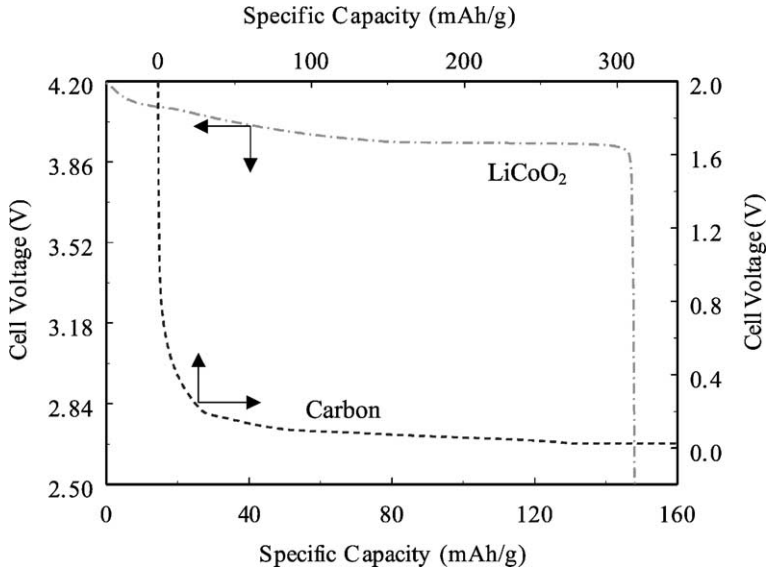

Fig. 2. OCP curves of positive ($LiCoO_2$) and negative (graphite) electrodes of Sony 18650 cells.

Table 1
Parameters for the positive and negative electrode materials

Symbol	Units	Anode (graphite)	Cathode ($LiCoO_2$)
L_i	μm	88	80
σ^{eff}	S/m	5.764	12.117
δ	μm	2	2
ε_2		0.485	0.385
c_1^{max}	mol/m^3	30555	51555
θ^0		0.74[a]	0.5
		0.83[b]	
D_1	m^2/s	3.9×10^{-14}	1.0×10^{-14}
k	(A/m^2)/(mol/m^3)$^{3/2}$	1.89×10^{-6}[a]	9.81×10^{-7}
		2.2×10^{-6}[b]	
α_a		0.5	0.5
α_c		0.5	0.5
c_2^0	mol/m^3	1000	
D_2	m^2/s	7.5×10^{-10}	
t^+		0.363	
R_f^o	Ω m^2	0.01	0

[a] Based on initial approach with all capacity loss attributed to carbon electrode.
[b] Based on fitting experimental half-cell data at low rates.

and the total theoretical capacity per unit area of the electrode material can be defined as

$$Q'_{th,i}\,(\mathrm{As/m^2}) = F \times C_{max,i} \times L_i, \quad i = \mathrm{n, p} \tag{14}$$

where C_{max} is the maximum concentration of the electrode in a phase which is the property of the material and is given by

$$C_{max,i}\,(\mathrm{mol/m^3}) = \frac{\rho_i}{\mathrm{MW}_i}, \quad i = \mathrm{n, p} \tag{15}$$

Based on the volume fraction of the phase, the maximum capacity available can be calculated as

$$Q_{max,i}\,(\mathrm{As/m^2}) = F \times \varepsilon_i \times C_{max,i} \times L_i \tag{16}$$

For a completely charged Li-ion cell, the negative electrode (graphite or coke) would be lithiated while the positive electrode ($LiMn_2O_4$ or $LiCoO_2$) would be de-lithiated. During discharge the Li-ions de-intercalate from the carbon and intercalate into the positive electrode through a highly conductive electrolyte ($LiPF_6$ in EC/DMC). Thus, during discharge, the state of charge of the negative electrode decreases while the state of charge of the positive electrode increases. Opposite will occur during charge. In general, the SOC of the negative and the positive electrode materials during discharge were estimated by using the following expressions:

$$\theta_n = \theta_n^o - \frac{i_{app}t}{Q_{max,n}}$$
$$\theta_p = \theta_p^o + \frac{i_{app}t}{Q_{max,p}} \tag{17}$$

where the initial values of SOC of negative (θ_n^o) and positive (θ_p^o) electrodes were given by

$$\theta_n^o = \frac{Q_n}{Q_{th,n}} \tag{18}$$

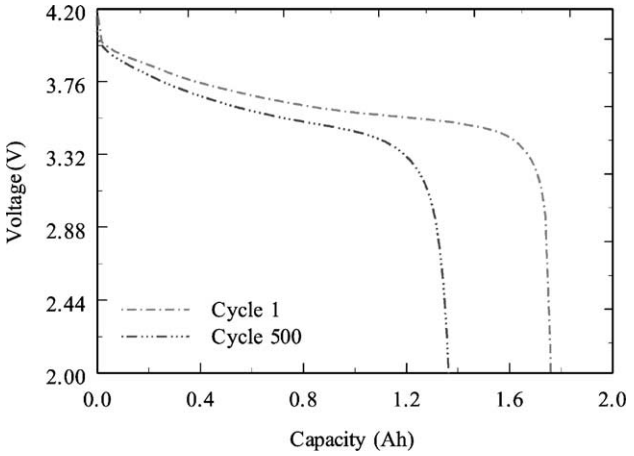

Fig. 3. Discharge curves of Sony 18650 cells for cycle numbers 1 and 500.

Thus, SOC of any electrode is defined as the measure of primary active material content in it. For example, the SOC of completely lithiated graphite material is 100% and it is 0% for completely de-lithiated one. For developing any capacity fade model, the parameters to be considered for accounting capacity loss with cycling are, SOC of the electrode material, maximum concentration in a phase, thickness of the electrode material and the volume fraction of the phase (solid/solution).

Capacity fade correlations in literature attribute the entire capacity fade during to the loss of the active material. Since C_{max} represents the property of the electrode material while the thickness and volume fraction depend on the preparation procedures, it would be a valid assumption to consider that the only variable that accounts for the capacity fade with cycling is the SOC. Since the negative electrode (carbon) limits the cell capacity, variations of lithiation capacity of negative electrode are considered for simulating capacity fade.

Fig. 3 shows the discharge performance of Sony 18650 cells initially and after 500 cycles. Two prominent changes observed in Fig. 3 are the decrease in the overall cell capacity and the increase in the voltage drop during discharge. In our model, the SOC of the negative electrode is considered for the first change namely the capacity loss with cycling. The second change, that is the drop in the cell voltage, is due to the increase in the cell resistance. It has been generally accepted that a number of unwanted side reactions occur during cycling. These reactions result in formation of products that passivate the surface of the electrode. For example, pure Li metal has a conductivity of (1.078×10^7 S/m), while one of the products (Li_2CO_3, formed as a result of solvent reduction during charging), has a very poor conductivity (1.2×10^{-6} S/m). Thus, it is necessary to introduce an additional term to the over-potential expression that will represent the potential drop at the interface due to presence of resistive film formed on the electrode particles. Thus, the over-potential can be represented as

$$\eta = \phi_1 - \phi_2 - U_{ref} - \frac{J}{a}R_f \tag{19}$$

Table 2
Values of θ_n and R_f for different cycle numbers

Cycle number	θ_n^N	R_f ($\Omega\,m^2$)
1	0.72	0.01
50	0.672	0.022
100	0.632	0.0245
150	0.62	0.0271
300	0.559	0.0365
500	0.514	0.044

The over-potential term given in Eq. (19) was used in the Butler–Volmer kinetic expression (Eq. (9)). In the semi-empirical model developed in this study, both the SOC and the film resistance of the negative electrode were used as an adjustable parameter to fit the experimental data for various cycle numbers.

The next step involves development of semi-empirical correlations for two capacity fade parameters used to predict the performance of the battery as a function of number of cycles. The Li-ion intercalation model was used for all simulations. By using two adjustable parameters (the state of charge and the resistance), the discharge curves (voltage versus time) were simulated using the intercalation model and were fitted with the experimental data. From this fitting, the state of charge (θ_n) and the film resistance (R_f) were extracted for different cycle numbers. Table 2 summarizes the values of θ_n and R_f used to fit the discharge curves for different cycles. Based on the variations of these parameter values, the following correlations were developed for the state of charge and resistance as a function of the cycle number.

The decrease in the SOC of the negative electrode with cycle number is fitted with a one-parameter correlation given by

$$\theta_n^N = \theta_n^o - k_1(\text{cycle})^{1/2} \tag{20}$$

where the constant k_1 depends on cycling conditions and the type of negative electrode material used. The square-root dependence for the cycle number can be accounted for by a parabolic growth mechanism for the continuous formation of a thin-film solid electrolyte interface (SEI) layer over the surface of the negative electrode.

The same type of semi-empirical correlation was found to be sufficient to explain the increase in the film resistance with cycling and is given by

$$R_f^N = R_f^o + k_2(\text{cycle})^{1/2}$$

where k_2 is a constant that and R_f^o is the resistance of the SEI layer. The values of the constants used in the semi-empirical correlations for the film resistance and for the SOC for two temperatures are given in Table 3. The variation of the adjustable parameters with cycling and the corresponding empirical fit are shown in Fig. 4. Based on these correlations, the capacity loss and the discharge performance could be predicted for any cycle number by assuming that the same trend follows all through cycling. Fig. 5 shows the simulated discharge curves for several cycles with the incorporation of the correlations developed for θ_n, R_f. For comparison, the experimental cycle data for cycle numbers 1 and 800 are also presented.

Due to a continuous increase in the film resistance during cycling, the rate capability of the cells decreases. After 500 cycles one observes a clear difference between the capacities obtained at very low rates of discharge ($<C/5$) and the capacity obtained with regular cycling rates ($C/2$, $1C$). The actual active material loss must be calculated by using only very low discharge rates. The difference in the capacity obtained at low and at high discharge rates will result in estimation of rate capability losses. Since in the above treatment, the entire capacity loss for $C/2$ rate cycling was accounted as an active material loss (SOC), the model results over predicted the capacity loss resulting from the active material. Thus, it is necessary to modify this model to account for the rate capability losses separate from the active material loss.

To further refine our present approach, the capacity loss with cycling is split to account for both, the active material losses and the rate capability losses. The solid phase diffusion coefficient of the limiting electrode is the adjusting parameter, which is used to determine the rate capability losses. The same empirical correlation used for the variation of film resistance with cycling is also used here.

In our previous work [9], we identified the following parameters to be critical in determining the capacity fade of Sony 18650 cells: the rate capability, secondary active material ($LiCoO_2$/Carbon) and primary active material (Li^+) losses. Thus, the total capacity fade as 'Q' can be quantified in terms of the three factors:

$$Q = Q_I + Q_{II} + Q_{III} \tag{22}$$

where Q_I represents the rate capability loss; Q_{II} the capacity loss due to secondary active material and Q_{III} refers to capacity loss due to primary active material. Thus, the model considers the following parameters: (i) the state of charge of

Table 3
Values of the constants of the semi-empirical correlations for film resistance, SOC and diffusion coefficient for two different cycling temperatures

Cycling temperature (°C)	Film resistance parameter	SOC parameters			Diffusion coefficient parameters	
	k_2 ($\Omega\,m^2$ per $cycle^{1/2}$)	θ^o (T)	k_3 ($cycle^{-2}$)	k_4 ($cycle^{-1}$)	k_5 (m^2/s)	k_6 (cycle)
25	1.5×10^{-3}	0.837	8.5×10^{-8}	2.5×10^{-4}	6.134×10^{-17}	1.25×10^{3}
50	1.7×10^{-3}	0.839	1.6×10^{-6}	2.9×10^{-4}	3.902×10^{-16}	6.91×10^{2}

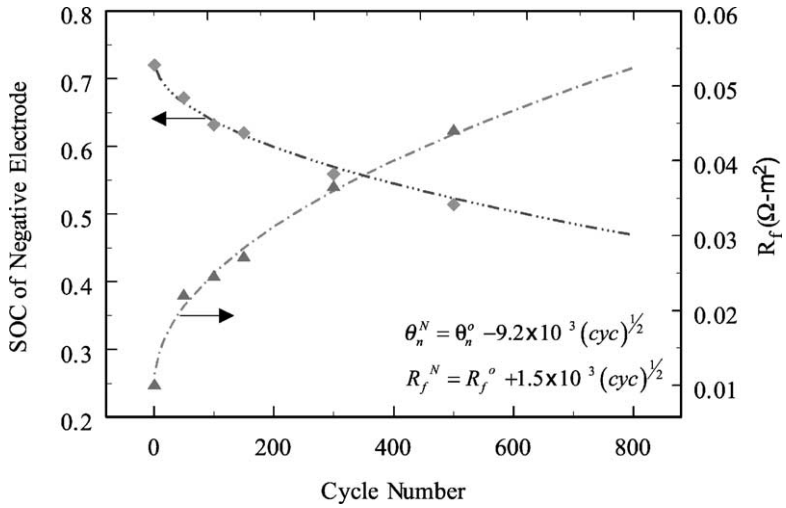

Fig. 4. Variation of the adjustable parameters θ_n and R_f with cycling and the respective empirical fits.

the limiting electrode which accounts for capacity loss due to primary and secondary active materials (Q_{II} and Q_{III}); (ii) solid phase diffusion coefficient of the limiting electrode to account for capacity loss due to rate capability (Q_I) and (iii) film resistance to account for the increase in the polarization and charge transfer resistance with cycling.

As a result of unwanted side reactions, there is a continuous loss of the active material for every charge/discharge cycle and hence the kinetic expression for active material losses could be written as SOC varying with cycle number. Since the negative electrode was limiting electrode all the SOC calculations were based on graphitic carbon. The initial state of charge of the negative electrode was estimated at very low discharge rate (~C/9) of a fresh cell. First, the specific capacity ($Q|_{C/9}$) was calculated, since the total amount of intercalation host material was known and the SOC was estimated by dividing the specific capacity with the theoretical capacity of graphitic carbon (372 mAh/g):

$$\theta_n^o = \frac{Q|_{C/9}}{Q_{th}} \tag{23}$$

From the active material losses (both primary and secondary) found experimentally for several cycle numbers, the loss in the SOC was calculated by

$$\theta_n^{lost} = \frac{Q_{lost}}{Q_{th}} \tag{24}$$

Here the term Q_{lost} includes both primary (Q_{III}) and secondary (Q_{II}) active material losses. Thus the SOC of the limiting electrode at any cycle number is given by

$$\theta_n^N = \theta_n^o - \theta_{lost} \tag{25}$$

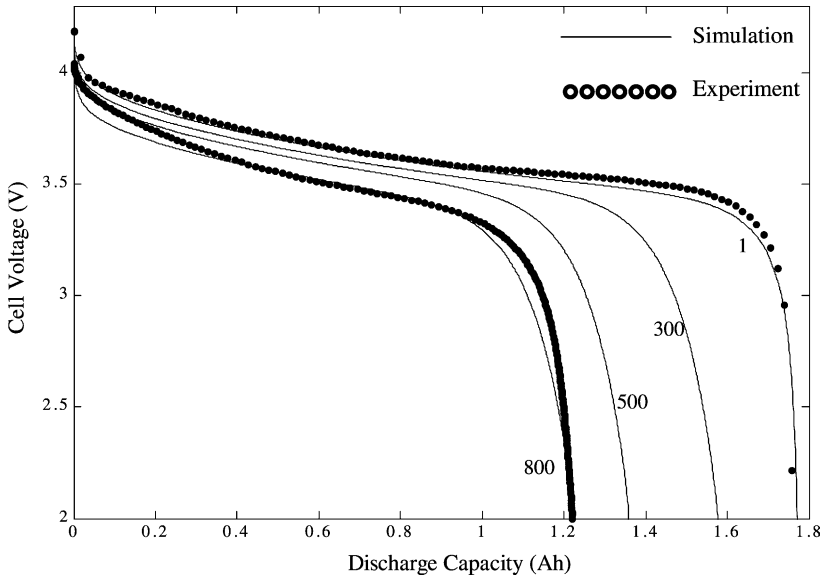

Fig. 5. Simulated discharge curves with the incorporation of empirical correlations for θ_n and R_f to the Li-ion intercalation model. The dotted curves represent the experimental data obtained for Sony 18650 cells for cycles 1 and 800.

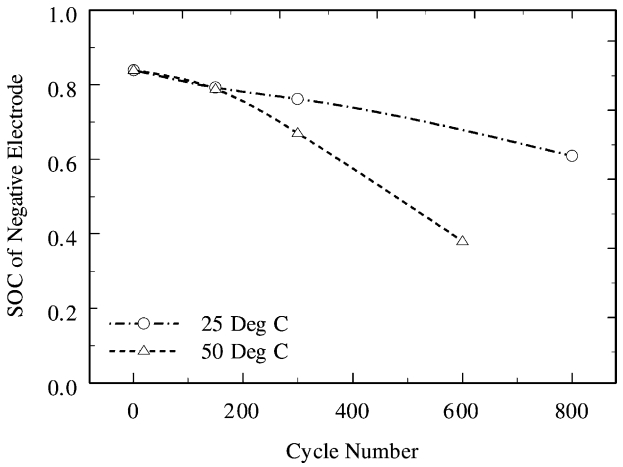

Fig. 6. Variation of SOC of negative electrode for the semi-empirical model with cycling at 25 and 50 °C.

The capacity loss was quantified experimentally for four cycle numbers (1, 150, 300 and 800) and hence the correlation for variation of SOC with cycling was developed based on these data. The rate of change of state of charge of electrode material is expressed as

$$-\frac{\mathrm{d}\theta_\mathrm{n}}{\mathrm{d}N} = k_3 N + k_4 \tag{26}$$

$$\text{initially} \quad \theta_\mathrm{n} = \theta^\mathrm{o}(T) \tag{27}$$

where N is the cycle number. Fig. 6 presents the semi-empirical fit based on Eqs. (26) and (27) for the variation of SOC of the negative electrode with cycling under different temperatures. The constant k_3 accounts for capacity losses that increase rapidly under adverse conditions such as cycling at high temperature and k_4 is a factor to account for capacity loss under usual conditions of charge and discharge. Table 3 summarizes the values for the constants k_3 and k_4 for cycling temperatures namely 25 and 50 °C. While the constant k_4 remains almost the same for both cases, the constant k_3, which was stated as a factor that's takes into account the cycling temperature, increases with increase in temperature. Based on the above rate expression it is possible to predict the capacity of the cell at any cycle number at lower rates of discharge. Still the rate capability losses and the polarization resistance need to be accounted to predict the discharge curve at any cycle as well as the cell capacity at moderate to high discharge rates.

The performance studies on Sony 18650 cells [9] clearly showed that the rate capability of the cells continues to decrease with cycling. The fresh cell showed only a small decrease in capacity with increase in discharge current indicating that the cell possesses a very good rate capability. Rate capability measurements after 150 and 300 cycles for the cells cycled at RT conditions showed similar profiles as that of the fresh cell. After 300 cycles there is a notable difference in discharge capacity obtained at low and high rates. For cycling at high temperatures (50 °C), rate capability limitations set in earlier.

Decrease in the rate capability with cycling could be explained based on the film formation over the electrode surface as a result of the side reactions. Li-ion diffuses in and out of the electro active material at slower rate as a result of a continuous film formation. Thus the rate capability could be treated as a diffusion limited problem and correlations can be developed for the change in diffusion coefficient with continuous cycling. This approach would be appropriate to get better predictions of discharge performance at moderate to high rates.

The diffusion coefficient of negative electrode and the film resistance were taken in this model as adjustable parameters. The experimentally obtained discharge curves for different cycles were fitted using the Li-ion intercalation model. From this fitting the value of diffusion coefficient and the resistance were extracted as a function of the cycle number. Next, using the correlation for variation of SOC with cycle number, the diffusion coefficient of negative electrode and the film resistance as adjustable parameters, the discharge curves were predicted for different cycle numbers.

As stated earlier, the capacity loss in the model was accounted by means of active material losses (Q_II and Q_III) in terms of SOC and rate capability losses (Q_II) in terms of diffusion coefficient. The drop in the cell voltage with cycling was accounted by adjusting the film resistance term that appears in the Butler–Volmer kinetic equation.

For cells cycled at RT conditions, the rate capability up to 300 cycles almost remains the same as that of the fresh cells. There was no significant difference in the discharge capacity obtained between very low rates of discharge ($C/9$) and the discharge rate used for cycling ($C/2$). The rate capability losses (capacity at $C/9$ − capacity at $C/2$) were estimated as 28 and 38 mAh after 150 and 300 cycles, respectively, which are comparable to the rate capability loss of 25 mAh for a fresh cell. Thus with the same value of diffusion coefficient, we were able to fit the discharge curves between cycles 1 and 300. Since the rate capability continues to diminish with continued cycling, the diffusion coefficient had to be adjusted or decreased to fit the other discharge curves (cycle numbers $>$ 300). Based on these observations, the correlation for variation of diffusion coefficient with cycle number was expressed as

$$D^\mathrm{s}_{\mathrm{n},N} = k_5 \exp\left(\frac{k_6}{N}\right) \tag{28}$$

where k_5 and k_6 are constants that are functions of both SOC and cycling temperature. Similar empirical correlation was developed for the cells cycled at 50 °C. Table 3 summarizes the values of the constants k_5 and k_6 for the two cycling temperatures. As shown in Table 3, the values of both constants increase with increase in cycling temperature.

The same correlation as used in the first approach for film resistance (R_f) was used in this model also in order to simulate the drop in cell voltage with cycling. Table 3

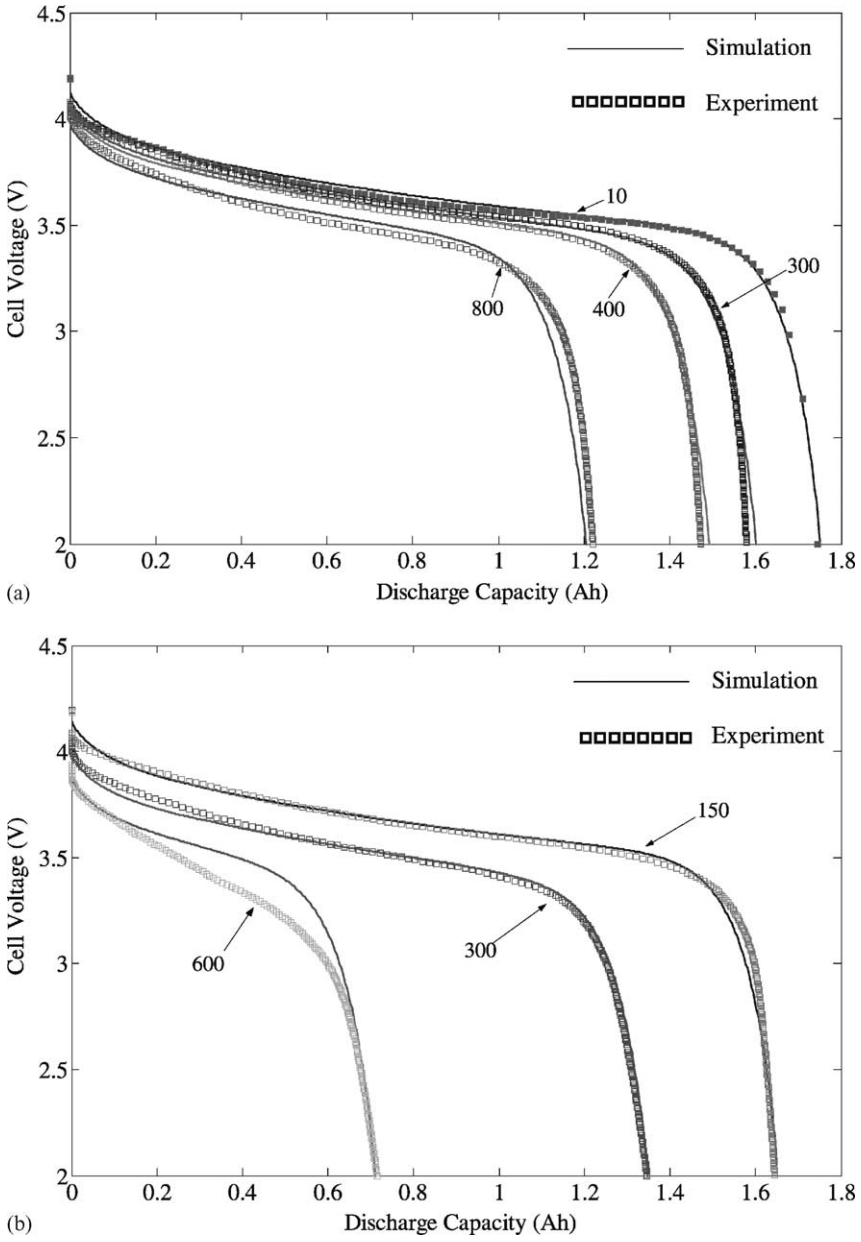

Fig. 7. Simulated discharge curves based on semi-empirical model for temperatures (a) 25 °C and (b) 50 °C. The dotted curves represent the experimental data obtained for Sony 18650 cells for the respective cycle numbers.

summarizes the values of the constant k_2 used for the two temperatures.

Fig. 7a and b presents the experimental discharge performance of Sony 18650 cells at various cycles discharged at 25 and 50 °C, respectively. Fig. 7a and b also show the model fits for comparison. The semi-empirical correlations obtained for the change of the state of charge, diffusion coefficient and the resistance as a function of cycle number were used to extract the parameters necessary for model predictions.

As shown in Fig. 7b, the accuracy of the fit diminishes with an increase of temperature. This phenomenon can be explained by taking into account that for simulating the battery performance at different cycles the same empirical expression for open circuit potential has been used. The error in fitting experimental curves at 50 °C indicates that the property of the intercalation host material changes with temperature that affects the shape of the OCP curve.

Fig. 8a and b show the capacity of Sony 18650 cells at different discharge rates. Discharge curves obtained from the semi-empirical model are compared to experimental data for different cycle numbers. This analysis has been done for two different temperatures namely, 25 and 50 °C. For all discharge rates between *C*/9 and 1*C*, a good fit was observed between the model results and the experimental data.

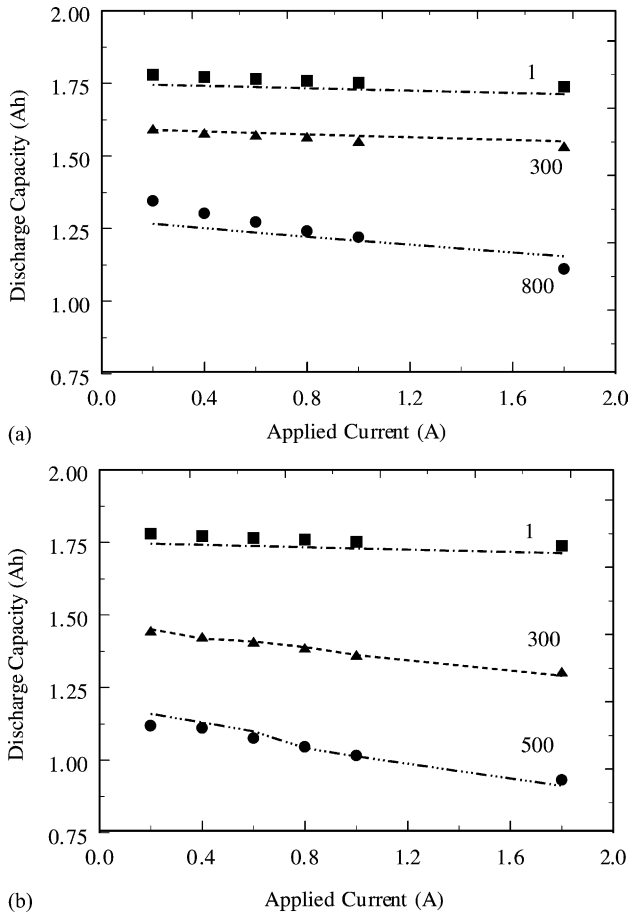

Fig. 8. Comparison of rate capability between experiment (dots) and model (solid lines) at various cycles for cells cycled at (a) 25 °C and (b) 50 °C.

While the model presented here can account for various capacity losses, it is still limited to the system for which empirical correlations were developed (Sony 18650 cells in this case). Similar correlations with different parameters will have to be derived for other battery geometries and electrode chemistries. In order to develop a generalized capacity fade model for Li-ion battery, it is necessary to use a first principles approach that takes into account the basic mechanism for capacity fade common to all Li-ion systems. The model should be capable of explaining the capacity loss under cycling conditions such as charging to several EOCV and discharging to different DODs and charging and discharging at different rates.

3. Conclusions

A semi-empirical capacity fade model has been developed for Li-ion cells. As a first step, empirical correlations were developed for state of charge and film resistance based on fitting the experimental data with Li-ion intercalation model. The entire capacity loss with cycling was assumed to be as a result of active material degradation and hence the capacity fade was correlated to the SOC. The capacity loss due to rate capability was not considered separately.

To account for rate capability, a charge balance was obtained through analysis of half-cell data of fresh and cycled cells. This model considered both the active material loss and the rate capability losses. Empirical correlations were developed for the change in SOC of negative electrode material based on experimental observations. Solid phase diffusion coefficient of the limiting electrode is the parameter considered to account for the rate capability losses. An empirical correlation for the variation of film resistance with cycling was used to explain the continuous increase in the cell voltage drop with cycling. With this approach the total capacity loss from both active material and rate capability losses were determined.

Acknowledgements

Financial support provided by National Reconnaissance Office for Hybrid Advanced Power Sources #NRO-00-C-1034 and National Science Foundation Grant #0097701 is acknowledged gratefully.

Appendix A

For the graphite electrode:

$$U_{\mathrm{n}}^{\mathrm{ref}} = 0.7222 + 0.1387\theta_{\mathrm{n}} + 0.029\theta_{\mathrm{n}}^{1/2} - \frac{0.0172}{\theta_{\mathrm{n}}} + \frac{0.0019}{\theta_{\mathrm{n}}^{1.5}} + 0.2808\mathrm{e}^{(0.90-15\theta_{\mathrm{n}})} - 0.7984\mathrm{e}^{(0.4465\theta_{\mathrm{n}}-0.4108)} \quad (A.1)$$

For the $LiCoO_2$ electrode:

$$U_{\mathrm{p}}^{\mathrm{ref}} = \frac{-4.656 + 88.669\theta_{\mathrm{p}}^2 - 401.119\theta_{\mathrm{p}}^4 + 342.909\theta_{\mathrm{p}}^6 - 462.471\theta_{\mathrm{p}}^8 + 433.434\theta_{\mathrm{p}}^{10}}{-1 + 18.933\theta_{\mathrm{p}}^2 - 79.532\theta_{\mathrm{p}}^4 + 37.311\theta_{\mathrm{p}}^6 - 73.083\theta_{\mathrm{p}}^8 + 95.96\theta_{\mathrm{p}}^{10}} \quad (A.2)$$

The solution phase conductivity as a function of concentration c_2 (in mol/dm^3) is [13]:

$$\kappa^{\mathrm{eff}} = \kappa\varepsilon_2^{4.0} = (4.1253 \times 10^{-4} + 5.007c_2 - 4.7212 \times 10^3 c_2^2 + 1.5094 \times 10^6 c_2^3 - 1.6018 \times 10^8 c_2^4)\varepsilon_2^{4.0} \quad (A.3)$$

References

[1] I. Bloom, et al., J. Power Sources 101 (2001) 238.
[2] T. Inoue, T. Sasaki, N. Imammura, H. Yoshida, M. Mizutani, in: Proceedings of the NASA Aerospace Battery Workshop, Huntsville, Alabama, 2001.

[3] P.D. Hafen, R.E. Corbett, in: Proceedings of the Intersociety Energy Conversion Engineering Conference, vol. 16 (1), 1981, p. 199.
[4] P. Bro, S.C. Levy, Quality and Reliability Methods for Primary Batteries, 1990, Wiley, NY, p. 127 (Chapter 10).
[5] C. Jordy, J.L. Liska, M. Saft, in: Proceedings of the 39th Conference on Power Sources, vol. 145, 1998, p. 1801.
[6] P. Ramadass, A. Durairajan, B.S. Haran, R.E. White, B.N. Popov, J. Electrochem. Soc. 149 (1) (2002) A54.
[7] P. Ramadass, B. Haran, R. White, B.N. Popov, J. Power Sources 111 (2002) 210.
[8] P. Ramadass, B. Haran, R. White, B.N. Popov, J. Power Sources 112 (2002) 606.
[9] P. Ramadass, B. Haran, R. White, B.N. Popov, J. Power Sources 112 (2002) 614.
[10] M. Doyle, T.F. Fuller, J. Newman, J. Electrochem. Soc. 140 (1993) 1527.
[11] T.F. Fuller, M. Doyle, J. Newman, J. Electrochem. Soc. 141 (1994) 1.
[12] P.M. Gomadam, J.W. Weidner, R.A. Dougal, R.E. White, J. Power Sources 110 (2002) 267.
[13] M. Doyle, J. Newman, A.S. Gozdz, C.N. Schmutz, J.-M. Tarascon, J. Electrochem. Soc. 143 (1996) 1890.